J. Fluid Mech. (1986), *vol.* 168, *pp.* 515–540
Printed in Great Britain

Oscillatory flows in wavy-walled tubes

By M. E. RALPH

Department of Applied Mathematics and Theoretical Physics, University of Cambridge, Silver Street, Cambridge CB3 9EW

(Received 22 October 1984 and in revised form 25 February 1986)

The problem of oscillatory viscous flow in a tube with rigid sinusoidal walls of large amplitude is solved numerically, for Reynolds numbers up to 300 and Strouhal numbers in the range 10^{-4}–1. Flow visualization photographs have confirmed qualitatively many of the predictions. Results analogous to those of Sobey (1980, 1983) for the two-dimensional problem have been obtained for regions of the parameter space studied in detail by that author. However, new flow structures are found in the previously neglected Strouhal number range of 0.02–0.1. These flows are characterized by significant interaction of flow events in successive half-cycles, due to the persistence of strong shed vortices. Bifurcation of the solution structure can then occur for Strouhal numbers between about 0.025 and 0.045, with the development of time-asymmetric flows: thus the velocity field at some instant of a positive-flow half-cycle may not be equal to minus the velocity field at the corresponding instant of a negative-flow half-cycle.

1. Introduction

In 1973, Bellhouse *et al.* reported on the success of a membrane oxygenator which utilized pulsatile flows across a furrowed membrane and gave good mass-transfer performance under laminar flow conditions. Bellhouse & Snuggs (1977) investigated this phenomenon in a flow visualization study. Steady flows and uniformly accelerating or decelerating flows were produced past a semi-cylindrical hollow in an otherwise flat wall, and two important observations were made: the vortices formed in accelerating flow were much stronger than those maintained in steady flow at the peak Reynolds number; and, during deceleration, the fluid comprising the vortex in the hollow was ejected far out into the main flow. The efficiency of the Bellhouse oxygenator was thus explained in terms of good lateral mixing.

The numerical study of Sobey (1980) and the experiments of Stephanoff, Sobey & Bellhouse (1980), on oscillatory flows in symmetrical wavy-walled channels, representing a more realistic model of the oxygenator, confirmed that vortices would be formed in the hollows as the flow accelerated; the centre of each vortex would then move towards the channel centreline as the flow decelerated and reversed in direction. Sobey (1980) also considered the low-Reynolds-number and high-Strouhal-number limits of wavy-walled channel flows, and the low-Strouhal-number limit was described in Sobey (1983). Asymmetrical channel flows were examined in Sobey (1982).

There have been a number of related numerical studies of unsteady internal flows with large wall perturbations: Cheng, Clark & Robertson (1972) and Cheng, Robertson and Clark (1973) considered oscillatory flows in channels with periodic, symmetric rectangular occlusions; Daly (1975, 1976) studied pulsatile flow past a single smooth constriction in an axisymmetric pipe; and Savvides & Gerrard (1984) considered

axisymmetric flows in tubes with triangular corrugations of the wall. A common finding of all these works is that a vortex expands as the mean flow decelerates, and its centre moves towards the axis of the conduit. Daly pointed out the possible physiological importance of this effect in thrombus dislodgement at an arterial stenosis, and Savvides & Gerrard have shown, by computing particle paths, that significant lateral motion of fluid particles accompanies vortex ejection.

The principal aim of the present work has been to provide, for axisymmetric conduits, a more comprehensive survey of the parameter space than has hitherto been given for oscillatory flow in any conduit with periodic wall shape. The steady-flow problem has been considered elsewhere (see Ralph 1985 for a survey of some of the recent literature). The paper is organized as follows: the numerical and flow visualization techniques are described in §§2 and 3; §4 deals briefly with the axisymmetric analogues of the flows described in Sobey (1980, 1983); several new flow structures are described in §§5 and 6, and in §7 the regions of the parameter space in which the various flows occur are summarized; some conclusions are given in §8.

2. Mathematical formulation and numerical solution

The formulation is similar to that of Sobey (1980), and is described in more detail in Ralph (1985). The axial and radial coordinates are $\hat{a}(x, r)$, (see figure 1), the corresponding velocity components are $\hat{U}_0(u, v)$ and the time, density, pressure and kinematic viscosity are $t/\hat{f}$, $\hat{\rho}$, $\hat{\rho}\hat{U}_0^2 p$, and $\hat{\nu}$ respectively, where $\hat{f}$ is the frequency of the time variation in flow rate. If $\hat{Q}_0$ is the maximum volumetric flow, then $\hat{U}_0$ is given by

$$\hat{U}_0 = \hat{Q}_0/\pi\hat{a}^2, \tag{1}$$

and the flow rate varies according to

$$\hat{Q} = \hat{Q}_0 \sin 2\pi t. \tag{2}$$

Hence for t between 0 and 0.5 the mean flow (or 'bulk' flow) is positive (taken to be the sense left to right) and for t between 0.5 and 1 it is negative. The mean flow has its maximum magnitude at the times $t = 0.25$ and 0.75.

The governing equations are the axisymmetric forms of the Navier–Stokes equations with zero azimuthal velocity (see Batchelor 1967, for example), here expressed in dimensionless form

$$\frac{\partial u}{\partial t}+\frac{1}{St}\left\{u\frac{\partial u}{\partial x}+v\frac{\partial u}{\partial r}\right\} = -\frac{1}{St}\frac{\partial p}{\partial x}+\frac{1}{\alpha^2}\left[\frac{\partial^2 u}{\partial x^2}+\frac{1}{r}\frac{\partial u}{\partial r}+\frac{\partial^2 u}{\partial r^2}\right], \tag{3}$$

$$\frac{\partial v}{\partial t}+\frac{1}{St}\left\{u\frac{\partial v}{\partial x}+v\frac{\partial v}{\partial r}\right\} = -\frac{1}{St}\frac{\partial p}{\partial r}+\frac{1}{\alpha^2}\left[\frac{\partial^2 v}{\partial x^2}+\frac{1}{r}\frac{\partial v}{\partial r}+\frac{\partial^2 v}{\partial r^2}-\frac{v}{r^2}\right], \tag{4}$$

and

$$\frac{\partial u}{\partial x}+\frac{v}{r}+\frac{\partial v}{\partial r} = 0. \tag{5}$$

St and α^2 represent a Strouhal number and a frequency parameter respectively, defined by

$$St = \frac{\hat{a}\hat{f}}{\hat{U}_0} \tag{6}$$

and

$$\alpha^2 = \frac{\hat{a}^2\hat{f}}{\hat{\nu}}. \tag{7}$$

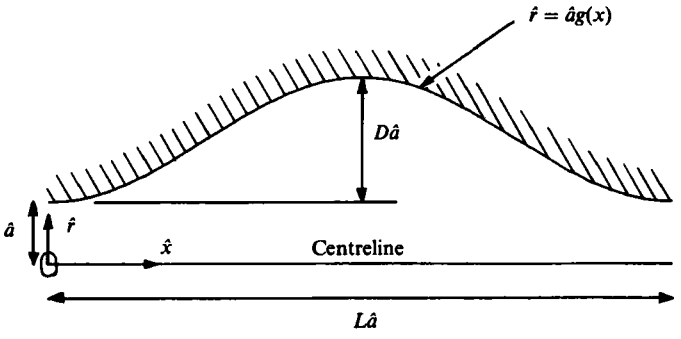

FIGURE 1. The geometry of the wavy-walled tube.

The ratio $\alpha^2/St = \hat{U}_0\hat{a}/\hat{\nu}$ will be denoted by Re_0, and represents the peak Reynolds number of the flow. The vorticity ζ and stream function ψ are defined by

$$\zeta = \frac{\partial v}{\partial x} - \frac{\partial u}{\partial r} \tag{8}$$

and

$$u = \frac{1}{r}\frac{\partial \psi}{\partial r}, \quad v = -\frac{1}{r}\frac{\partial \psi}{\partial x}. \tag{9a, b}$$

The governing equations are then recast as a vorticity transport equation and a Poisson equation for the stream function. Following Sobey (1980), a Prandtl-type transformation is made to simplify application of the boundary conditions:

$$z = rh(x), \tag{10}$$

where

$$h(x) = \frac{1}{g(x)} \tag{11}$$

and $g(x)$ is a function representing the shape of the wall (see figure 1). In the present work $g(x)$ has taken the form

$$g(x) = 1 + \tfrac{1}{2}D\left[1 - \cos\frac{2\pi x}{L}\right], \tag{12}$$

and the parameters D and L have been given the values 2 and 10 respectively. The coordinates are further transformed, departing from Sobey's formulation, by defining

$$y = z^2 \tag{13}$$

so that for equal increments in y, the increments in z and r are smaller near the walls than near the axis of the tube. The rationale for this transformation is that it is thought to be desirable to concentrate mesh points at the wall, where the vorticity gradients are largest. The system of governing equations obtained by applying the two transformations is as follows:

$$\frac{\partial \zeta}{\partial t} = -\frac{1}{St}\left\{u\frac{\partial \zeta}{\partial x} + 2\left[y\left(\frac{h'}{h}\right)u + hy^{\frac{1}{2}}v\right]\frac{\partial \zeta}{\partial y} - \frac{h}{y^{\frac{1}{2}}}v\zeta\right\} + \frac{1}{\alpha^2}\left\{\nabla^2\zeta - \frac{h^2}{y}\zeta\right\} \tag{14}$$

and

$$\nabla^2\psi = 4h^2\frac{\partial \psi}{\partial y} - \frac{y^{\frac{1}{2}}}{h}\zeta, \tag{15}$$

where a prime denotes differentiation with respect to x and

$$\nabla^2 \equiv \frac{\partial^2}{\partial x^2} + 4y\left(\frac{h'}{h}\right)\frac{\partial^2}{\partial x\,\partial y} + 4y\left[y\left(\frac{h'}{h}\right)^2 + h^2\right]\frac{\partial^2}{\partial y^2} + \left[4h^2 + 4y\left(\frac{h'}{h}\right)^2 + 2y\left(\frac{h'}{h}\right)'\right]\frac{\partial}{\partial y} \quad (16)$$

u and v are given by

$$u = 2h^2\frac{\partial \psi}{\partial y} \quad (17)$$

and

$$v = -\frac{h}{y^{\frac{1}{2}}}\left[\frac{\partial \psi}{\partial x} + 2y\left(\frac{h'}{h}\right)\frac{\partial \psi}{\partial y}\right], \quad (18)$$

and the boundary conditions are

$$\psi|_{y=0} = 0, \quad (19)$$

$$\psi|_{y=1} = \tfrac{1}{2}\sin 2\pi t, \quad (20)$$

$$\zeta|_{y=0} = 0, \quad (21)$$

$$\zeta|_{y=1} = 8h\left[h^2 + \left(\frac{h'}{h}\right)^2\right]\left.\frac{\partial^2 \psi}{\partial y^2}\right|_{y=1}, \quad (22)$$

$$\psi|_{x=x_0+L} = \psi|_{x=x_0}, \quad (23)$$

$$\zeta|_{x=x_0+L} = \zeta|_{x=x_0}, \quad (24)$$

where x_0 denotes an arbitrary axial position. Equations (23) and (24) represent conditions of periodicity, implying that the solutions are valid only at some distance from the ends of the tube.

The above problem was represented in finite-difference form and a fairly standard algorithm, as described in Roache (1976), for example, was used to obtain solutions. Equation (14) was represented using centred-time, centred-space differences, with the Dufort–Frankel substitution, following Cheng *et al.* (1972, 1973) and Savvides & Gerrard (1984). Upwind differencing, which has a formal truncation error one order lower than central differencing but is less prone to numerical instability, has been used in the present work only in certain of the very low-Strouhal-number calculations described in §4. At each time step, the Poisson equation for the stream function was solved by an over-relaxation method with over-relaxation parameter 1.72.

A finite-difference grid with 41 axial and 17 radial mesh positions was used (except at very low values of Strouhal number when a 31×13 grid was utilized), and figure 2 shows the positions in the real geometry of computational mesh points which were uniformly spaced in the (x, y)-coordinate system. The quadratic stretching can be seen to result in a high resolution of the wall region at the expense of a rather coarse grid near the axis of the tube.

The extent of the parameter space has precluded the computation of each solution with a variety of grid sizes, but results for a single steady-flow test problem, using meshes with between 21×9 and 61×25 points, showed the solution to be convergent with decreasing mesh size. The Reynolds number in this test case was 200, of the same order of magnitude as the largest Reynolds number considered. The difference between the 'converged' value of the calculated mean pressure gradient and the value obtained with the 41×17 grid was about 3 %. With upwind differencing the error in this calculated parameter was greater than 25 %.

A further consideration regarding the accuracy of solutions concerned the dimen-

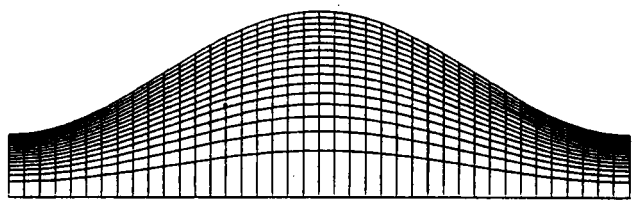

FIGURE 2. Location of computational mesh points in the (x, r)-coordinate system.

sionless time for which a given computation had to be continued in order that the transient effect of time-marching the solution from rest should become negligible. When transient effects had decayed, the velocity field at any instant was usually identical with that at the corresponding instant in the previous half-cycle, except for a change of sign. The 'settling time' was found to increase with α^2, so that for values of α^2 of order unity, computation of about 1.5 cycles was sufficient to obtain periodicity in time, whereas for values of order 10, about 6 cycles were required. A solution was said to be 'periodic in time' when streamline patterns at corresponding instants in successive half-cycles were precise mirror images, within the limits of plotting accuracy. In certain flows, half-cycle periodicity was never established, but the streamline patterns at corresponding instants of successive complete flow cycles became identical. In other cases the flow could only be said to be periodic when three complete flow cycles were considered, or else periodicity was not established at all within the limits of the computation time. Flows which did not show half-cycle periodicity are described in §6.

The size of the timestep was determined by stability considerations, and typical values were in the range 1.25×10^{-3} to 5×10^{-4}. Values as small as 3×10^{-5} were required in the very low-Strouhal-number flows.

3. Flow-visualization experiments

Flow visualization in axisymmetric geometries is complicated by the fact that the material of the tube wall and the fluid itself can act as a strong lens. This prevents more than a fraction of the plane which it is intended to view from being held in focus, and also tends to scatter the incident light. To overcome these problems, the exterior of the test section should be rectangular, and it is also desirable to match the refractive indices of the working fluid and the material of which the test section is made.

In the present work, oil of turpentine was used as the working fluid (with a refractive index of about 1.47), and the test section was constructed from Perspex (of refractive index about 1.49). The test section was made in two halves, by pressing a male mould into two blocks of Perspex which were subsequently machined and polished: this gave a square exterior cross-section. The test section consisted of five complete wall wavelengths with minimum bore 4 mm, maximum bore 12 mm and wavelength 20 mm [corresponding to $L = 10$ and $D = 2$ in (12)]. 200 mm of straight, uniform tube of 4 mm bore carried the flow at each end of the test section.

Flows were made visible by injecting into the working fluid highly reflecting particles of mica and titanium dioxide, sold commercially as 'Mearlin' (Mearl Corporation, N.Y.), which were illuminated on an axial plane. The particles were 5–90 μm in size, and although not neutrally buoyant, the terminal velocities were very

small compared with the fluid velocities and cannot have significantly affected the visualization photographs. Illumination was provided by a 150 W projector light source, collimated through a pair of slits.

Oscillatory flows were induced using a variable-speed d.c. motor to drive a piston via a variable-stroke Scotch-yoke mechanism. A small magnet mounted on the flywheel of the motor passed over a Hall-effect switch fixed to the baseplate, and the signal from the switch was output to an electronic timing unit [previously used in the experiments of Stephanoff *et al.* 1980]. The timing unit was used to trigger the camera through a motor drive unit, and allowed for a variable delay between the Hall switch pulse, representing a reference phase position, and the opening of the camera shutter. The camera used was a Nikon F-2, with 55 mm Micro-NIKKOR lens, MD-2 motor drive unit and PB-5 bellows focusing unit. Kodak 2475 recording film was used at the maximum aperture setting of f 3.5.

In oscillatory flows, particle paths do not in general coincide with streamlines, but if the exposure time is short compared with the timescale for significant changes in the streamline pattern, there will be approximate coincidence over the exposure time. From this point of view it was desirable to use as short an exposure as possible. However, a lower limit on exposure time was imposed by the need for an adequate exposure level, and hence there was an upper limit on the frequency of flows which could be studied, giving a maximum allowable value of α^2 of about 6. Exposure times of $\frac{1}{30}$ s and $\frac{1}{60}$ s were used. There was also an upper limit of about 0.05 on permissible Strouhal numbers: at larger Strouhal numbers the time required for a fluid particle to trace a path sufficiently long that its direction could be determined was too large a fraction of the flow period.

4. 'Intermediate' Strouhal number, viscous dominated and quasi-steady flows

In Sobey (1980, 1983), a number of oscillatory flow structures occurring in symmetrical wavy-walled channels were described, and these have been found to have their analogues in wavy-walled tube flows. Further description of the axisymmetric flows is given in Ralph (1985), but a brief review of their most important features is given here for completeness and for comparison with the new flow patterns detailed subsequently.

Figure 3 shows computed instantaneous streamlines in an axisymmetric flow with parameters $Re_0 = 50$ and $St = 0.005$, corresponding to the 'intermediate' Strouhal-number category of Sobey (1980). Figure 3 (a) depicts the streamlines at $t = 0.07$, that is at a time early in the acceleration phase of the flow cycle, when there is no flow separation. An incipient separation region is present at $t = 0.10$ (figure 3b) which grows to occupy most of the hollow at the instant of peak flow (figure 3c). The vortex continues to grow in size as the flow decelerates (figure 3d), so that at the time of zero flow, a large recirculation is present (figure 3e). The flow close to the wall already being in the negative sense, when the bulk flow changes sign, fluid passes between the wall and the vortex rather than along the centreline, giving the streamline pattern of figure 3(f) at time $t = 0.55$. The separation region on the axis is rapidly eroded, so that at time $t = 0.57$, the streamline pattern is identical with that in figure 3 (a), but with the flow in the opposite sense. Flow-visualization experiments have confirmed the occurrence of this flow structure in wavy-walled tubes.

At low Reynolds numbers (less than about 12 for the geometry considered here), the streamline patterns are similar to those shown in figure 3, but with flow reversal

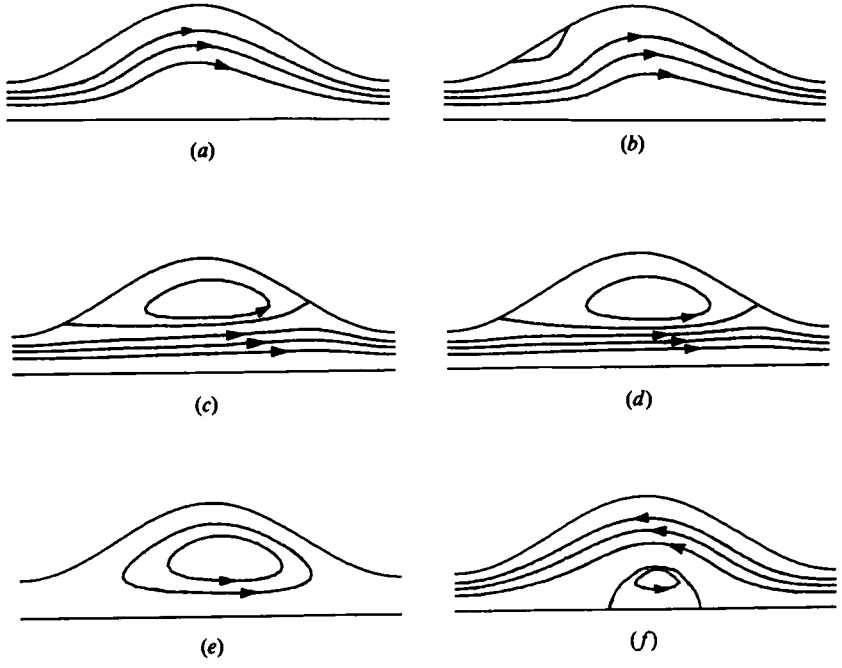

FIGURE 3. Computed instantaneous streamline plots for a flow with parameters $Re_0 = 50$, $St = 0.005$: (*a*) $t = 0.07$; (*b*) 0.10; (*c*) 0.25; (*d*) 0.45; (*e*) 0.50; (*f*) 0.55.

occurring late in the deceleration phase of the flow cycle, and initiated at the tips of the hollows rather than in the diverging part of the tube. Sobey (1980) showed that this was because the flow is effectively governed by the unsteady Stokes equations, with the steady inertial terms exerting negligible influence on the flow structure. This is also true for relatively large Strouhal numbers (of order unity) at arbitrary Reynolds number.

At small values of Strouhal number and frequency parameter, the flow might be expected to become increasingly quasi-steady in character. However, as for flow in a uniform channel or tube, even if the frequency parameter is very small, there is always a time interval containing the time of mean-flow reversal when the flow is distinctly non-quasi-steady. Sobey (1983) proposed a definition of quasi-steadiness for wavy-walled channel flows which required that the inertially dominated separation region formed during bulk-flow acceleration should die away completely before the onset of viscous-flow reversal. He found that the upper limit on Strouhal number for quasi-steady flow was inversely proportional to the square of the Reynolds number, and this has also been found to be true for wavy-walled-tube flow.

5. Certain new flow structures in the Strouhal-number range 0.02–0.1

The Strouhal-number range 0.02–0.1 has not been investigated in detail previously, but there is a rich solution structure in this part of the parameter space.

5.1. *'Bursting through' of an ejected vortex and secondary separation*

Sobey (1980) observed that the initiation of a new separation region, as in figure 3(*b*), could occur before erosion of the old, ejected vortex (figure 3*f*) was complete. He

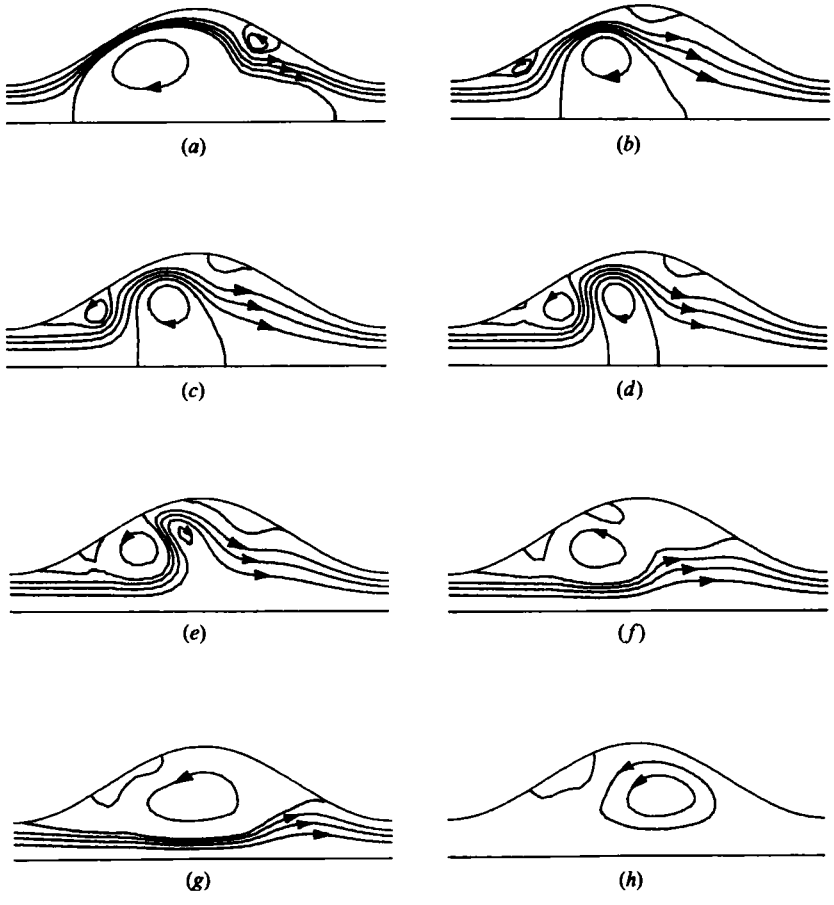

FIGURE 4. Computed instantaneous streamline plots for a flow with parameters $Re_0 = 200$, $St = 0.02$: (*a*) $t = 0.05$; (*b*) 0.20; (*c*) 0.25; (*d*) 0.30; (*e*) 0.35; (*f*) 0.40; (*g*) 0.45; (*h*) 0.50.

stated that in his computations, the velocity field due to the eroding vortex exerted little influence on the developing flow pattern. The present calculations have shown however, that if the Strouhal number is increased to values of about 0.02 or greater, the time required for erosion of the ejected vortex at the centreline increases dramatically, so that this vortex may continue to affect the flow development throughout the half-cycle following its ejection. One example of such a flow is shown in figure 4, in which the parameters take the values $Re_0 = 200$ and $St = 0.02$.

Figure 4(*a*) shows the flow early in the acceleration phase, with a large clockwise vortex at the centreline and a separation of opposite sign at the wall. A new counterclockwise separation occurs in the diverging part of the tube (figures 4*b*, *c*), in which secondary separation subsequently occurs (figure 4*d*). In figure 4(*e*), the flow 'bursts through' the vortex at the centreline before completely eroding it, resulting in a free toroidal vortex. Note that the flow is in the sense left to right at every point of the centreline in the figure, and hence there is a saddle point in the stream-function field. The free vortex attaches to the wall, and the streamlines straighten out as this saddle point disappears (figure 4*f*). At this instant, the new counterclockwise vortex coalesces with the old vortex of the same sign. There are then two clockwise vortices embedded in the main counterclockwise separation region, and these correspond to

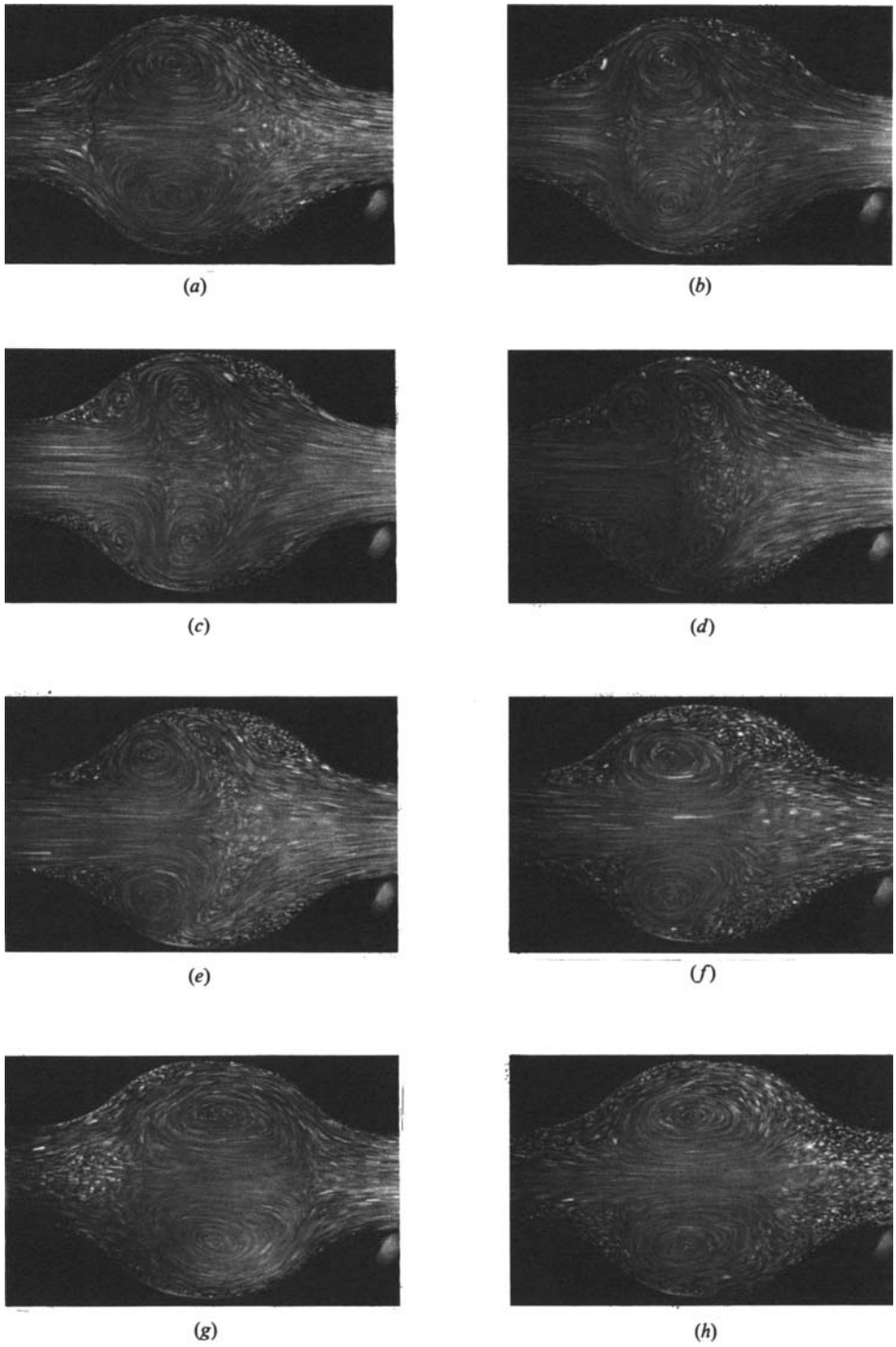

FIGURE 5. Flow-visualization photographs for a flow with parameters $Re_0 = 200$, $St = 0.02$: (*a*) $t = 0.05$; (*b*) 0.20; (*c*) 0.25; (*d*) 0.30; (*e*) 0.35; (*f*) 0.40; (*g*) 0.45; (*h*) 0.50.

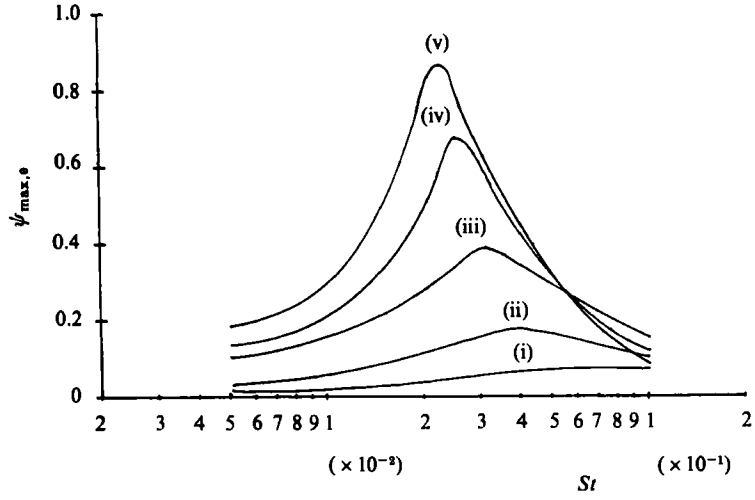

FIGURE 6. Variation of the vortex strength at times of zero flow with Strouhal number for various Reynolds numbers: (i) $Re_0 = 10$; (ii) $Re_0 = 20$; (iii) $Re_0 = 50$; (iv) $Re_0 = 100$; (v) $Re_0 = 200$.

the secondary separation of the present half-cycle and the main vortex of the previous half-cycle, persisting at much reduced size and strength. These vortices coalesce to form a single secondary separation region (figure 4*g*) before the instant of zero flow (figure 4*h*).

Visualization photographs obtained for the same values of the flow parameters are shown in figure 5, at times in the flow cycle corresponding to those of figure 4. The agreement is good, although any secondary separations present in figures 5(*f–h*) are rather too weak to be clearly discernible.

When secondary separation was observed at lower Reynolds numbers, this usually occurred near the time of peak flow, and the secondary-separation zone subsequently disappeared without affecting the flow structure significantly. Secondary separation in unsteady flow has been predicted by Gillani & Swanson (1976) for an isolated axisymmetric dilatation and by O'Brien (1975) in a symmetrical driven cavity flow. There is a striking similarity between O'Brien's flow structure and that just described: in both cases a primary vortex gives rise to a secondary separation which then coalesces with a new vortex of the same sign, formed after the flow direction reverses.

In order to understand certain changes in the flow structure as the governing parameters change, it is useful to consider the variations in strength of the recirculations formed. A measure of the vortex strength at the instants of zero flow is given by the maximum value of the stream function ψ_{max} at times $t = n$, where n is an integer (or equivalently the minimum value of the stream function at times $t = n+0.5$). Where two vortices are present ψ_{max} represents the strength of the one formed in the half-cycle immediately preceding the zero-flow instant. ψ_{max} is shown as a function of Strouhal number for various Reynolds numbers in figure 6. The essential features of the figure are the monotonic increase in ψ_{max} with Reynolds number at fixed Strouhal number over most of the Strouhal-number range, and the existence of an increasingly sharp maximum with respect to Strouhal number as the Reynolds number increases. The increase of vortex strength with Reynolds number is not surprising, but the effect of Strouhal number requires some explanation. It seems that at low Strouhal number the vortex strength is approximately governed

by quasi-steady considerations and is therefore relatively small, except near the time of mean-flow reversal, when viscous effects prevent the development of a strong vortex. As the Strouhal number increases at fixed Reynolds number, there is less time for diffusive cancellation of vorticity, and the vortex strength increases. At still higher Strouhal numbers, a different limiting mechanism becomes important, in that vorticity is confined to increasingly thin Stokes layers at the wall, and hence does not give rise to a strong vortex. Alternatively, the high-Strouhal-number limit can be seen as the result of a decrease in the importance of the nonlinear effects responsible for separation.

In the light of figure 6, the change in flow structure from that of figure 3 to that of figure 4 becomes more comprehensible. It can be seen that although figures 3(*e*) and 4(*h*) are qualitatively quite similar, the strength of the vortex in the latter figure is about eight times that in the former. In addition, values of α^2 and St are greater for the flow in figure 4, so that the times required for significant diffusive cancellation and convection of vorticity are increased. Hence the vortex tends to persist for a greater proportion of the flow cycle after its ejection. At a Strouhal number of 0.02, convective inertial effects are still important however, so that the rapid changes in the direction of the main flow shown in figure 4(*d*), for example, can only be sustained whilst the vortex remains very strong. When this strength is reduced somewhat, the high pressure at the stagnation point causes the main flow to burst through.

5.2. *Persistence of an ejected vortex*

If the Strouhal number is increased further, to values of about 0.05, figure 6 shows that vortex strengths tend to be lower than those considered in §5.1. However, the reduced rate of vorticity transport, compared with that at lower Strouhal numbers, means that an ejected vortex can persist throughout the half-cycle following its ejection. The reduced magnitude of convective inertial effects leads to the main flow passing around this vortex, which remains at the centreline, rather than bursting through it.

Streamline patterns in such a flow are shown in figure 7, in which the parameters take values $Re_0 = 120$ and $St = 0.05$. There are two vortices present at time $t = 0.05$ (figure 7*a*) of markedly different sizes and opposite signs. The larger vortex at the axis of the tube has been formed in the previous half-cycle, whilst the smaller one was formed in the half-cycle before that. This small vortex occupies a toroidal volume, but is not attached to the wall, along which the vorticity has the same sign everywhere. The small vortex rapidly disappears (figure 7*b*) but the streamlines remain 'kinked' throughout the remainder of the half-cycle as the fluid which comprised the vortex tends to retain its vorticity as it moves downstream.

A new flow separation occurs in the diverging part of the tube just before the instant of peak flow (figure 7*e*), and this region grows as the flow decelerates, exactly as for the flow in figure 3. The shape of the growing vortex reflects the fact that the entrained fluid possesses significant vorticity. Late in the deceleration phase, separation is also initiated in the converging part of the tube (figure 7*j*).

The most important new feature of the flow is the persistence of a vortex at the centreline throughout a half-cycle. The size of the vortex decreases at first (figures 7*a*–*d*), but then increases late in the deceleration phase (figures 7*j*, *k*), and when the flow comes to instantaneous rest, a pair of counter-rotating vortices occupies the hollow (figure 7*j*). The direction of flow is right to left on that part of the centreline occupied by the older (clockwise) vortex, and so as the mean flow accelerates in this

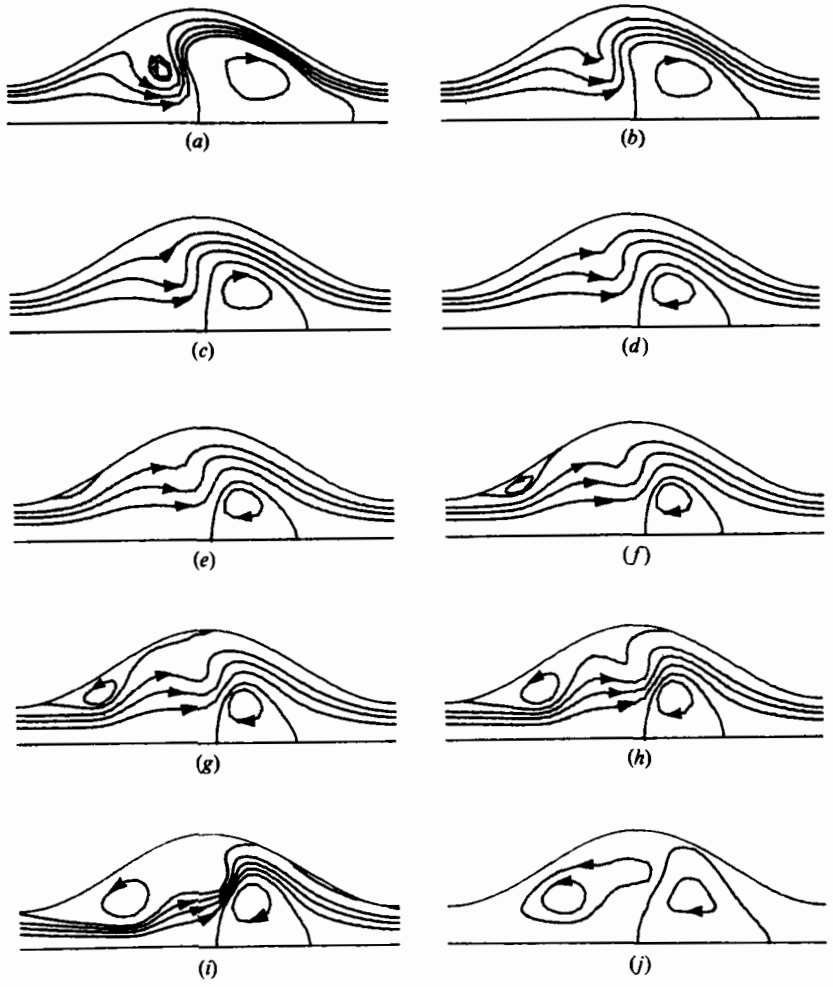

FIGURE 7. Computed instantaneous streamline plots for a flow with parameters $Re_0 = 120$; $St = 0.05$: (a)–(j) $t = 0.05$–0.50 in increments of 0.05.

sense, fluid passes through the middle of the vortex. The flow near the wall is also in the sense right to left, so a free toroidal vortex results as in figure 7 (a).

Flow-visualization experiments have confirmed the occurrence of flows of the kind just described, and photographs for a flow with the same parameter values as in figure 7 are given in figure 8. The agreement is generally good, although certain of the photographs show slight departure from axisymmetry. Additional understanding of the flow can be gained from consideration of instantaneous vorticity contour plots, and those corresponding to the streamline plots of figure 7 are given in figure 9. In each case, zero-vorticity contours are shown as dashed lines (but note that the vorticity is also zero on the axis), and the signs of the vorticity in adjacent regions are indicated on the figures. Magnitudes of contour increments are denoted by $\Delta\zeta_+$ and $\Delta\zeta_-$ in the positive- and negative-vorticity regions respectively. A striking feature of figure 9 is the persistence of a zone of negative vorticity in the right-hand half of each hollow, corresponding to the continued existence of a clockwise vortex. The magnitude of the vorticity minimum continues to decrease throughout the half-cycle however,

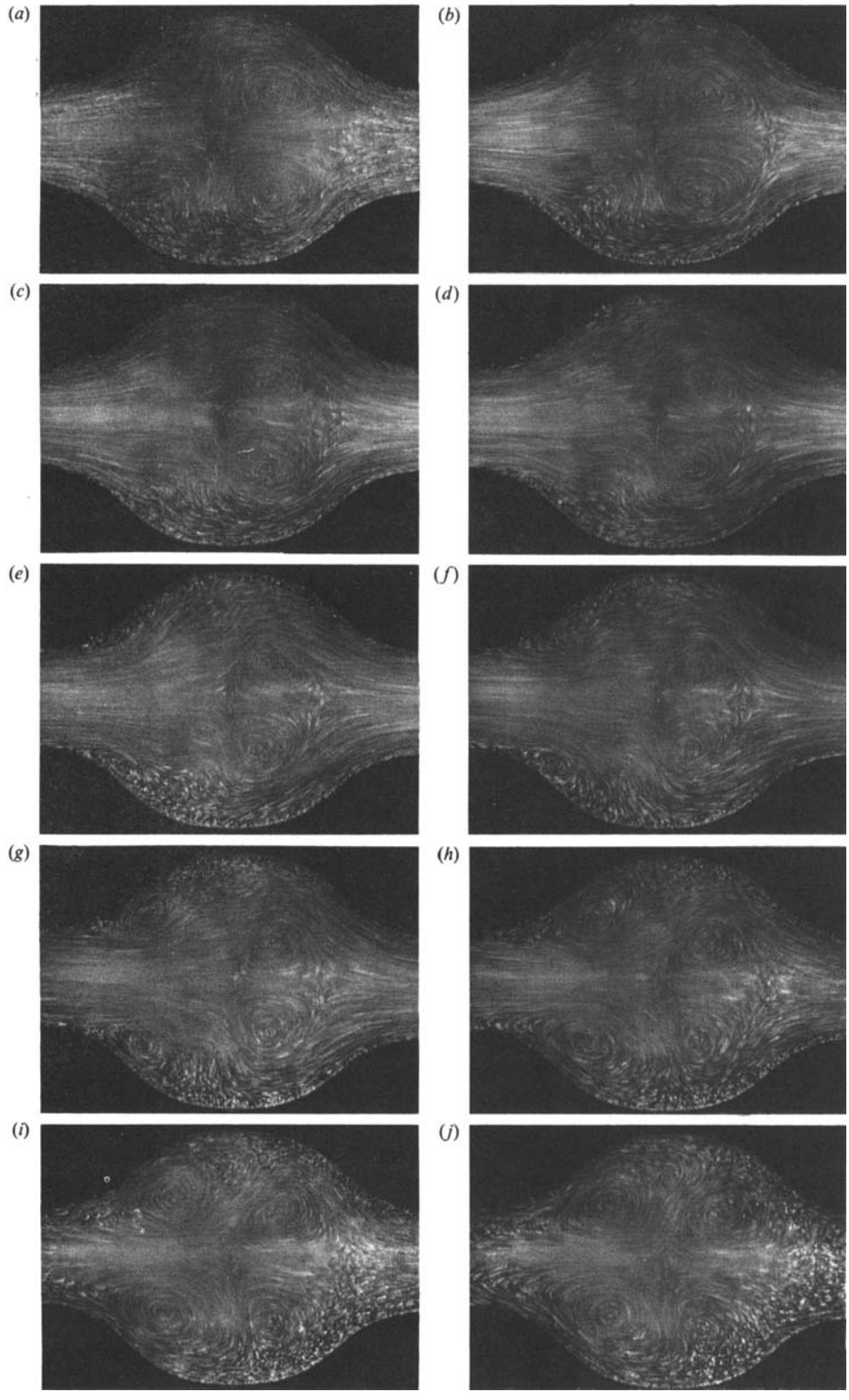

FIGURE 8. Flow-visualization photographs for a flow with parameters $Re_0 = 120$, $St = 0.05$: (*a*)–(*j*) $t = 0.05$–0.50 in increments of 0.05.

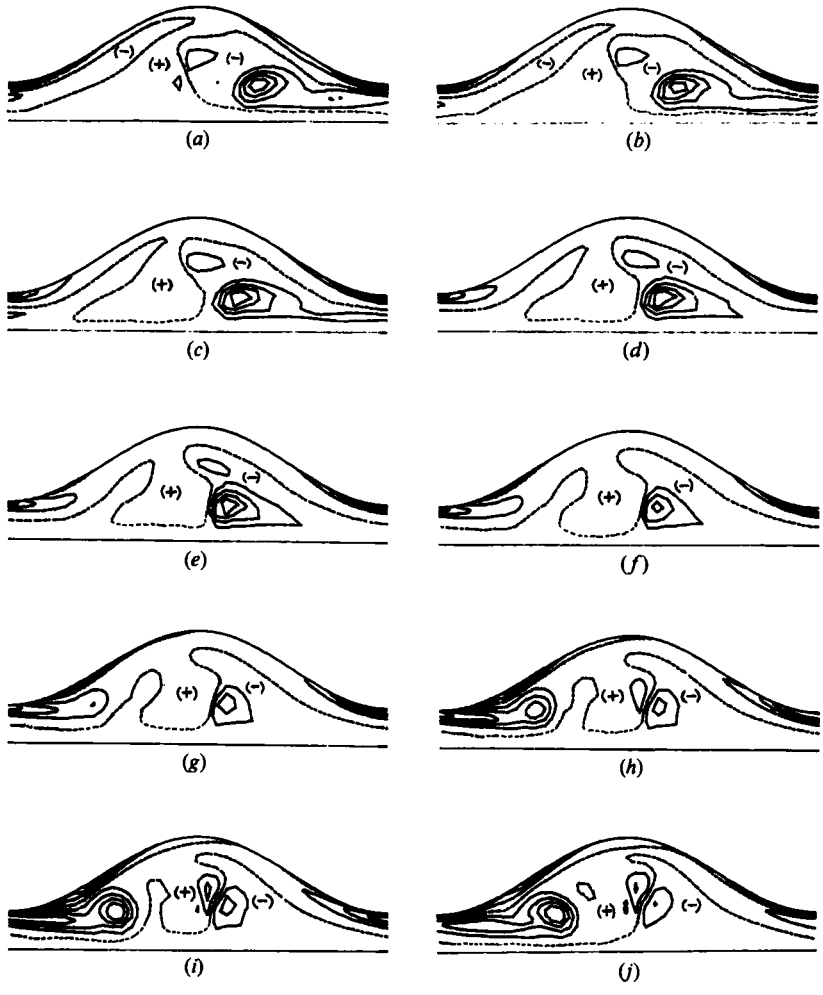

FIGURE 9. Computed vorticity contour plots for a flow with parameters $Re_0 = 120$, $St = 0.05$: (*a*)–(*j*) $t = 0.05$–0.50 in increments of 0.05: (*a*) $\Delta\zeta_+ = 1.09$, $\Delta\zeta_- = -0.49$; (*b*) 1.48, −0.45; (*c*) 1.82, −0.38; (*d*) 2.01, −0.36; (*e*) 2.02, −0.35; (*f*) 1.80, −0.49; (*g*) 1.34, −0.59; (*h*) 0.73, −0.61; (*i*) 0.54, −0.56; (*j*) 0.50, −0.66.

even when the separation region is expanding. The reduction occurs both by diffusive cancellation of vorticity at the centreline and by convection, but the latter mechanism is likely to be of secondary importance after the vortex reaches its minimum size and fluid from it ceases to be entrained by the main flow. Another important aspect of the vorticity plots is that the left and right halves of the hollow tend to be dominated by positive and negative vorticity respectively, because fluid particles near the cross-sections of maximum area are convected rather short distances.

Certain particle paths in a flow of this kind have been computed by numerical Lagrangian integration of the velocity field, and the results are shown in figure 10. The paths shown, which are typical of a larger set of results, are described over five complete flow cycles, beginning at an instant of zero flow. The figures suggest that there is relatively little fluid exchange through the cross-sections of maximum area, although there is good mixing within a wall wavelength centred at a constriction. If we consider the local Strouhal number at an enlargement, based on the mean

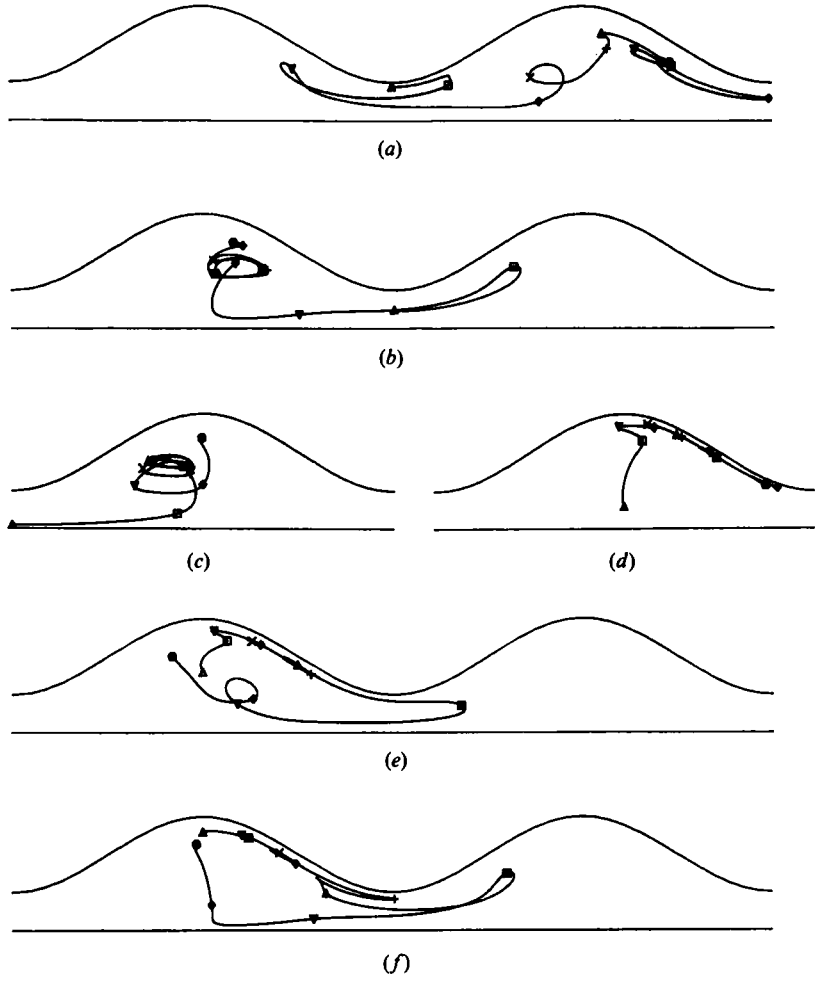

FIGURE 10. Some particle movements over five cycles in a flow with $Re_0 = 100$, $St = 0.05$: $t = 0$ (△); 0.5 (□); 1.0 (▽); 1.5 (◇); 2.0 (×); 2.5 (+); 3.0 (▲); 3.5 (■); 4.0 (▼); 4.5 (◆); 5.0 (●).

velocity there at an instant of peak flow, and on the local radius, this is 27 times greater than the Strouhal number defined in (6), based on conditions at a constriction, and is thus of order unity in figures 7–10. Hence we expect particles near an enlargement to be convected a dimensionless distance of this order during a cycle, with the result that positive vorticity, generated most strongly at a constriction during a positive 'stroke', is convected into the adjacent half-wavelength of the tube but not much further. The fact that any tube half-wavelength thus tends to contain vorticity of a particular sign at all times leads to steady streaming of the kind described by Lyne (1971) and by Hall (1974), with particles in the right-hand half of each hollow tending to describe clockwise paths, and those in the left-hand half describing counterclockwise paths.

At Strouhal numbers intermediate between those giving rise to the flows of figures 4 and 7, another flow structure has been predicted computationally, and this is shown in figure 11. The flow parameters take the values $Re_0 = 200$ and $St = 0.035$. The flow is similar to that of figure 7, but whereas the counterclockwise vortex of figure 7 (*a*) is rapidly eroded, that in figure 11 (*a*) reattaches to the wall (figure 11 *b*) and persists

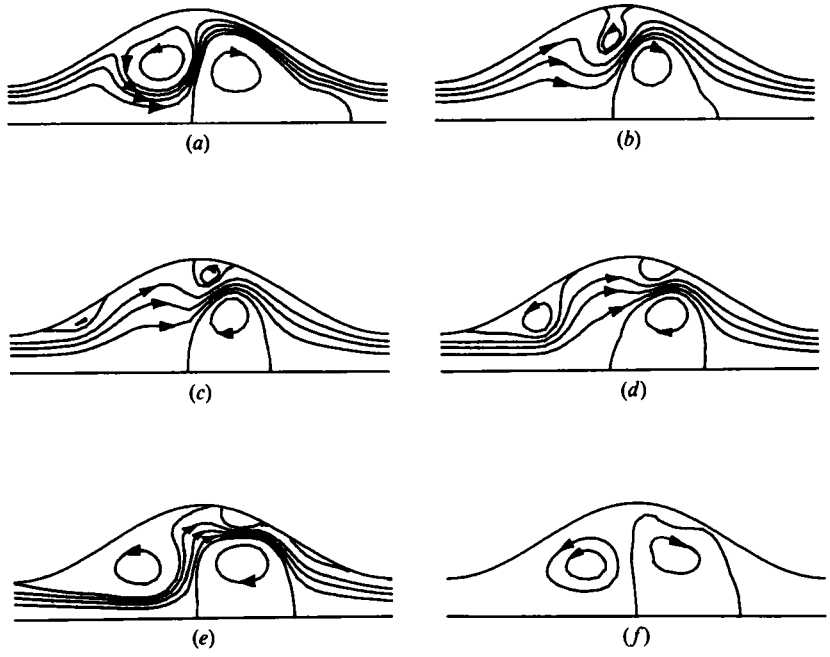

FIGURE 11. Computed instantaneous streamline plots for a flow with parameters $Re_0 = 200$, $St = 0.035$: (*a*) $t = 0.05$; (*b*) 0.15; (*c*) 0.25; (*d*) 0.35; (*e*) 0.45; (*f*) 0.50.

throughout the subsequent half-cycle. Note that the vortex strength at the time of zero flow is greater in the flow of figure 11 than in that of figure 7. However, the flow just described has not been observed experimentally, and is superseded by time-asymmetric flows of the kind described in §6. Possible reasons for this discrepancy are discussed in §6.3.

5.3. *Formation of a region of reversed flow at the centreline*

At Strouhal numbers somewhat greater than those considered in §5.2, flow structures of the kind shown in figure 12 result, in which the parameter values are $Re_0 = 50$ and $St = 0.08$. (The change in Reynolds number is less significant, as is shown in §7.) Figures 12 (*a–f*) show superficial similarity with the flow of figure 3, in that complete erosion of the ejected vortex at the centreline takes place, and a new separation occurs in the diverging part of the tube. Expansion of the new vortex takes place as the flow decelerates. A novel effect is shown in figure 12 (*g*) however, as a region of reversed flow is formed at the axis, so that at the instant of zero flow a pair of counter-rotating vortices occupies the hollow (figure 12 *h*). As the mean flow accelerates right to left, the clockwise vortex is rapidly eroded in the manner of figures 7 (*a*, *b*).

The change in flow structure occurring as the Strouhal number increases above values of about 0.05 can be related to the variation in vortex strength shown in figure 6. In figures 12 (*d–f*), although the flow is in the sense left to right at every point of the axis, there remains a negative vorticity peak at the site of the eroded vortex. As long as the flow rate remains close to its maximum value, this vorticity peak is not sufficiently strong to cause flow reversal. In the late stages of bulk-flow deceleration however, the slowest-moving fluid, which is that nearest the axis, reverses its direction of motion. This effect is analogous to that occurring in uniform tubes, at intermediate values of the frequency parameter, when the velocity profiles typically

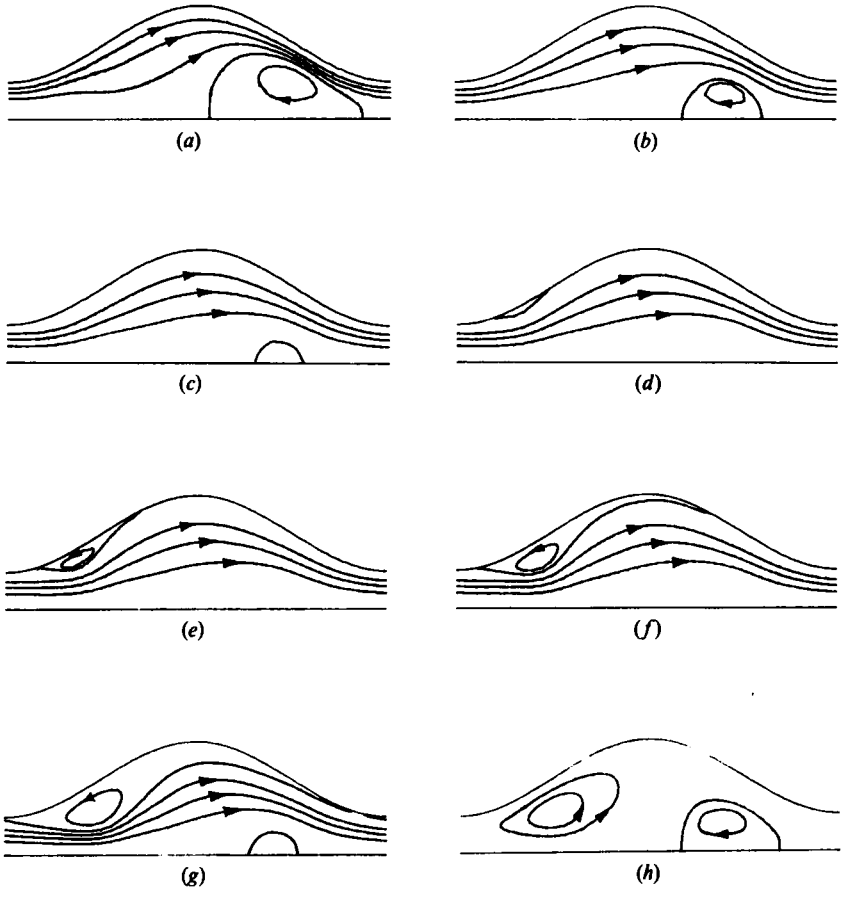

FIGURE 12. Computed instantaneous streamline plots for a flow with parameters $Re_0 = 50$, $St = 0.08$: (*a*) $t = 0.05$; (*b*) 0.15; (*c*) 0.25; (*d*) 0.30; (*e*) 0.35; (*f*) 0.40; (*g*) 0.45; (*h*) 0.50.

exhibit a maximum near the tube wall: in the wavy-walled-tube case this leads to the formation of closed streamlines. Thus, as the Strouhal number increases from values of about 0.05 to about 0.08, the time required for erosion of the vortex decreases, owing to the weakening of the recirculation: but the vortex reappears because of the slower rate of vorticity transport from the site of the erosion.

Unfortunately, flows of this kind were beyond the Strouhal-number range obtainable with the experimental apparatus.

6. Flows showing time asymmetry

In all of the flow structures discussed so far, a description of the velocity field as it varied over half of a flow cycle was sufficient to specify the flow completely, because the velocity field at any time t was precisely minus that existing at $t \pm 0.5$ (within the limits of numerical error). This is expected given the spatial and temporal symmetry of the imposed boundary conditions. Under certain conditions however, the solution develops time asymmetry as described below.

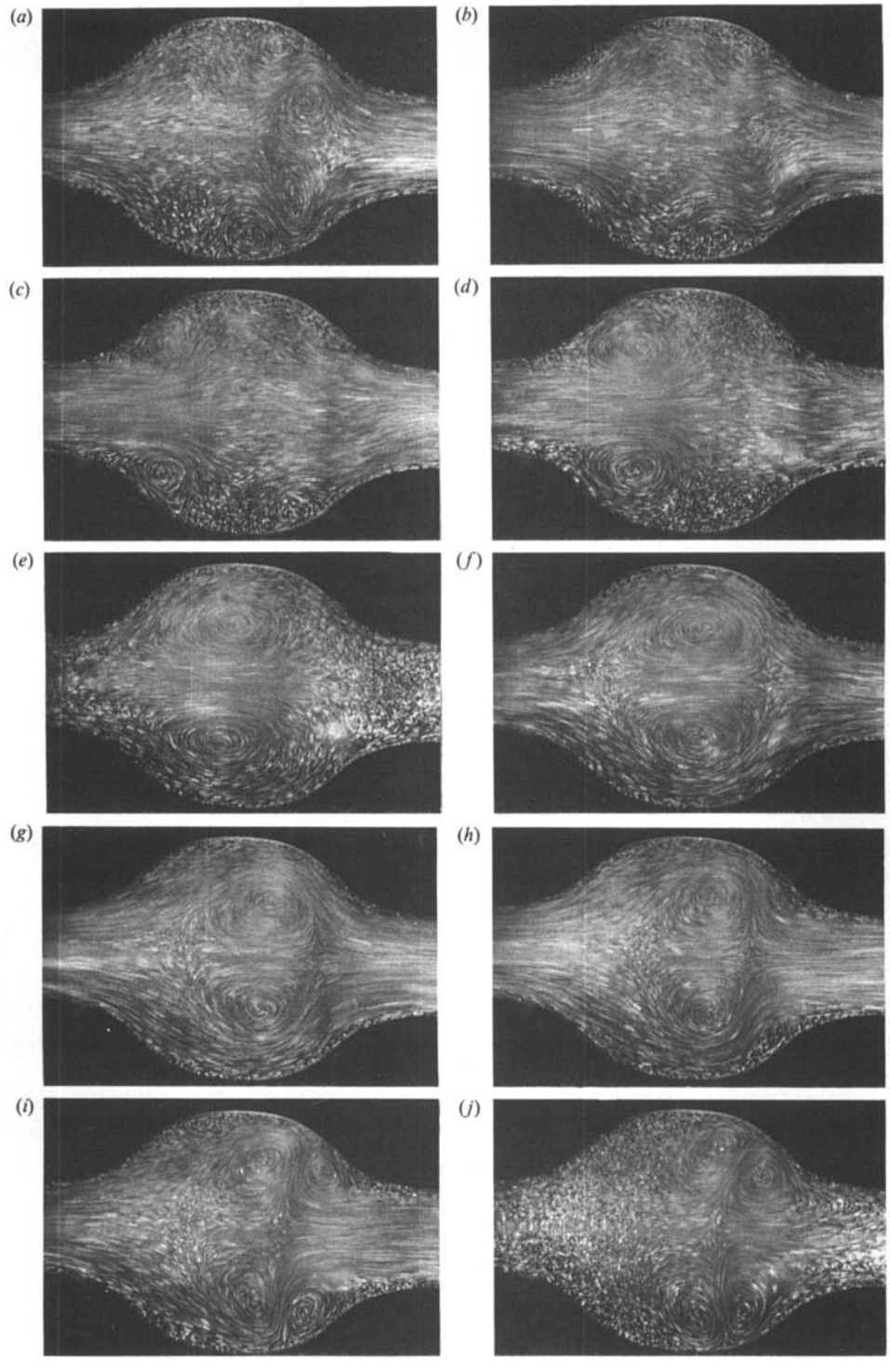

FIGURE 13. Flow-visualization photographs for a flow with parameters $Re_0 = 160, St = 0.035$: (a)–(j) $t = 0.10$–1.00 in increments of 0.10.

6.1. *Asymmetric effects in flow-visualization experiments*

Visualization photographs for a flow with $Re_0 = 160$ and $St = 0.035$ are shown in figure 13, in which the bulk flow is in the direction left to right in figures 13(*a–d*), is in the direction right to left in figures 13(*f–i*), and is instantaneously zero in figures 13(*e, j*). The time-asymmetry can be seen immediately from figures 13(*e, j*), since the former shows a single large vortex occupying the whole hollow, whilst the latter shows a pair of comparably sized vortices.

In figure 13(*a*) the flow is beginning to accelerate in the positive sense. A clockwise vortex occupies the right-hand part of each hollow near the axis, and a counterclockwise vortex is also present, nearer the wall. (Here and throughout this description the sense of rotation refers to that part of the axially symmetric recirculation visible in the upper half of each photo.) Both recirculations shrink in size initially, the counterclockwise vortex towards the hollow tip and the clockwise one towards the axis, where some departure from axisymmetry occurs (figure 13*b*). A new counterclockwise separation occurs at the wall, grows in size as the flow decelerates (figures 13*c, d*), and appears to have coalesced with the older vortex of the same sign at the time of zero flow. The centreline vortex has been completely eroded in this time.

As the flow accelerates right to left, the vortex which is now at the centreline is eroded much more slowly than that in figures 13(*a, b*) (figures 13*f, g*) and indeed persists until the next instant of zero flow. During this time, a new clockwise separation is initiated (figure 13*h*) which grows throughout the deceleration phase (figures 13*i, j*), but never occupies more than about one third of the hollow cross-sectional area. Note that a counterclockwise recirculation persists throughout the flow cycle, but that there are intervals when no recirculation of the opposite sense is present.

Observation of an unexpected time asymmetry of the kind just described raised the question as to whether this was simply an experimental artifact, and the experimental procedure was therefore examined in detail. The 'sense' of the asymmetry was found not to depend on the way in which the flow was started from rest: that is if, at the end of a piston stroke in one direction, a 'push' stroke say, a single vortex was present in a hollow (as in figure 13*e*), and at the end of a 'pull' stroke there was a pair of vortices, then this would be true for any start-up procedure. The test section had been designed so that the flow in the three central hollows was visible, and it was found that the sense of asymmetry in one of these hollows (at one end of the group of three) was different from that in the other two. This suggested that the sense of asymmetry was linked to small variations in wall shape. Belief in this hypothesis was strengthened when the orientation of the test section relative to the piston was reversed and the sense of asymmetry in each hollow remained fixed relative to the test section.

The occurrence of time asymmetry was thus linked to imperfections in the construction of the test section. However, for three reasons the asymmetric flow structure was not regarded simply as an artifact. First, the accuracy of the test-section shape was comparable with that which might be found in an engineering device (for example, the maximum variation in the bore at the contractions was about ± 0.1 mm with mean 4 mm). Secondly, for flows outside the Strouhal-number range of about 0.025–0.045, the experimental flow patterns showed no time asymmetry, suggesting that amplification of wall-shape inaccuracies occurs selectively. Finally, time-asymmetric flow structures have been predicted computationally, albeit with a higher Reynolds-number threshold.

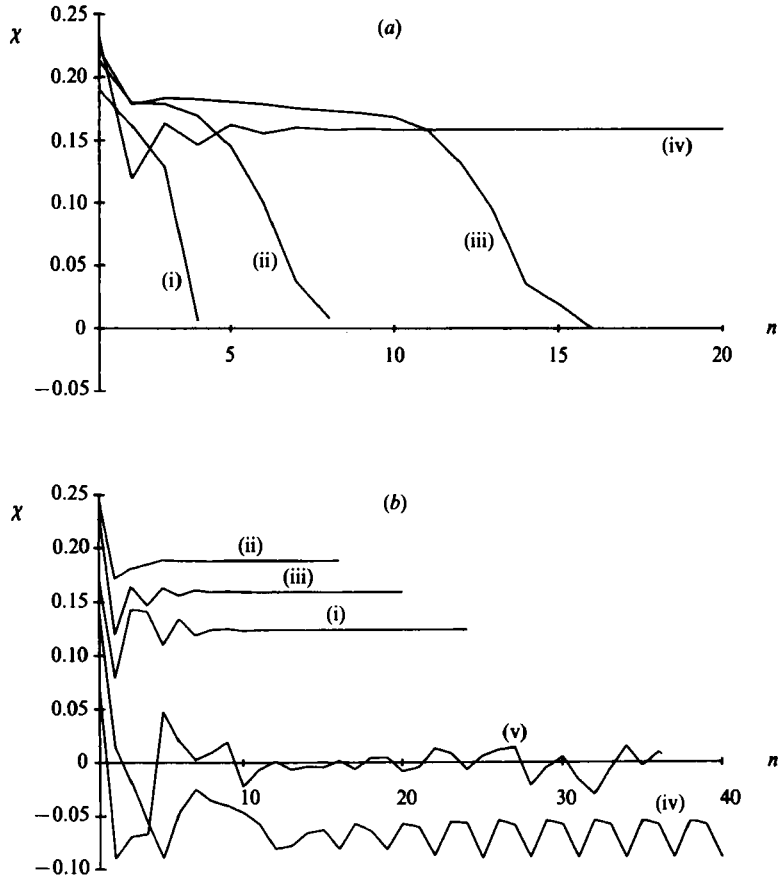

FIGURE 14. The relative asymmetry of the flow cycle as a function of the number of computed cycles. (*a*) $St = 0.035$: (i) $Re_0 = 160$; (ii) $Re_0 = 200$; (iii) $Re_0 = 220$; (iv) $Re_0 = 300$. (*b*) $Re_0 = 300$: (i) $St = 0.025$; (ii) $St = 0.030$; (iii) $St = 0.035$; (iv) $St = 0.040$; (v) $St = 0.045$.

6.2. *Asymmetric effects in computations*

In an attempt to quantify time-asymmetric effects in wavy-walled-tube flow, the relative amounts of vorticity present at the times of zero flow have been calculated. $|\bar{\zeta}|_n$ is defined as the sum of the magnitudes of the vorticity values at all computational nodes at time $t = n$, divided by the number of nodes; $|\bar{\zeta}|_{n+0.5}$ is the same quantity evaluated at time $t = n+0.5$. n is a positive integer representing the number of complete flow cycles computed, in a calculation in which the velocity is everywhere zero initially. Hence χ, given by

$$\chi = \frac{|\bar{\zeta}|_{n+0.5} - |\bar{\zeta}|_n}{|\bar{\zeta}|_{n+0.5} + |\bar{\zeta}|_n},$$

is a measure of the departure from symmetry of the velocity fields at the times of zero flow, and can be taken to represent the asymmetry of the overall flow structure. A non-zero value of χ is a sufficient condition for an asymmetric flow cycle, and experience shows that it is also a necessary condition in the present problem.

Figure 14(*a*) shows the variation of χ with n for a fixed Strouhal number, $St = 0.035$, and a variety of Reynolds numbers. It can be seen that for a relatively

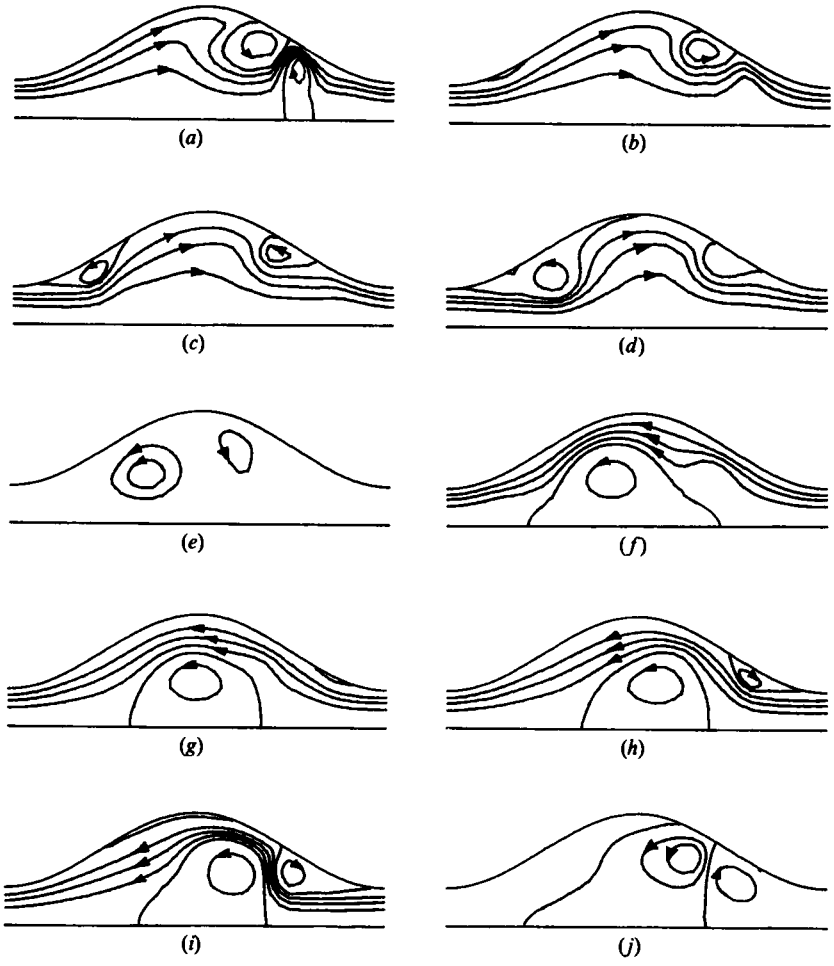

FIGURE 15. Computed instantaneous streamline plots for a flow with parameters $Re_0 = 300$, $St = 0.035$: (*a*)–(*j*) $t = 0.10$–1.00 in increments of 0.10.

low Reynolds number, $Re_0 = 160$, which nevertheless gives rise to asymmetrical flow in the visualization experiments, the degree of asymmetry decays fairly rapidly to negligible values. For lower-Reynolds-number flows the decay is even more rapid. As the Reynolds number increases however, the asymmetry persists for an increasing number of flow cycles, until for a Reynolds number of 300, χ reaches a uniform value within about 10 cycles and ceases to change further. A flow in which χ maintained the same value, correct to 5 significant figures, for 4 consecutive cycles was deemed to be permanently asymmetric.

The asymmetry of the flow at a Reynolds number of 220 decays in a distinctly non-uniform way, with a relatively gradual change in χ for n between 2 and 10, followed by a more abrupt decay. It appears that the asymmetry is nearly self-sustaining until it reaches a certain critical state, at which point it fails rapidly. The final flow structure is similar to that shown in figure 11, but up to $n = 10$, streamline patterns are like those in figure 13.

The variation of χ with n for a number of values of Strouhal number is shown in figure 14(*b*), in which the Reynolds number is 300. For Strouhal numbers of 0.025,

0.03 and 0.035, permanent asymmetry, under the definition given in the previous paragraph, occurs, whilst for Strouhal numbers of 0.02 or less and 0.05 or greater the asymmetry decays to a negligible level within a few cycles. Interesting behaviour is shown for $St = 0.04$ and 0.045. In the former case the flow appears to be time asymmetric, but with the degree of asymmetry varying with a period of three flow cycles; in the latter, χ varies in an apparently random fashion even after 36 complete flow cycles.

A set of computed streamline plots typical of the simpler asymmetric structures (that is, excluding the cases showing three-cycle periodicity or 'random' behaviour) is shown in figure 15, with the parameters taking values $Re_0 = 300$ and $St = 0.035$. These plots represent the 'settled' solution, so that the given non-dimensional times are relative to some time $t = n_0$, where n_0 is an integer not less than about 12. Despite the difference in Reynolds numbers, the flow structure is similar to that shown in the photographs of figure 13. Discrepancies arise in the precise shape of streamlines, and certain particular differences include the secondary co-rotating vortex in figure 15(*e*) which is not reflected in figure 13(*e*). Attempts at flow-visualization photography for the parameter set of figure 15 were unsuccessful because of the high α^2 limit described in §3, but visual observation suggested that the flow was similar to that of figure 15.

It has been noted that in every case in which asymmetry is predicted [excluding the cases of figure 14*b* (iv) and (v)], the sense of the asymmetry has been such that a single sense of recirculation is present after a positive 'stroke' and a pair of counter-rotating vortices after a negative stroke.

6.3. *Discussion of asymmetric flows*

Important questions arise from the discovery of time-asymmetric flows. These concern the causes of such asymmetries and the reason for their different Reynolds-number thresholds in the computations and experiments. The first question consists of two parts, in that the mechanisms both for triggering and maintaining the asymmetry must be considered.

Vorticity plots for the flow of figure 15 are shown in figure 16. The flow asymmetry is reflected in these plots primarily by the fact that the vorticity near the centreline is positive at all times, whilst negative vorticity tends to be concentrated nearer the wall. Such a distribution could be stably maintained as follows. The existence of a strong concentration of positive vorticity at the centreline leads to the persistence of a counterclockwise recirculation there. The right-to-left flow which generates negative vorticity is thus forced around this obstructing vortex, carrying negative vorticity only into the wall region. This in turn means that there is no strong clockwise vortex at the centreline and hence the left-to-right flow passes near the axis of the tube, and carries more positive vorticity there. Figures 16(*c–g*) show a positive vorticity peak being generated at a constriction and transported from there to a position near the middle of a hollow, whereas no equivalent transport process is apparent in figures 16(*j*, *k*, *a*, *b*).

The mechanism just described depends critically on the values of the flow parameters, since asymmetries are only found in a limited region of the parameter space. In particular, it is necessary to generate a counterclockwise vortex of sufficient strength to persist at the centreline for some time following its ejection. The Strouhal-number range in which asymmetric effects occur corresponds approximately with that giving rise to the strongest vortices.

The ways in which asymmetric flows are triggered, as opposed to maintained, appear to be different in the experiments and computations, since the determinant

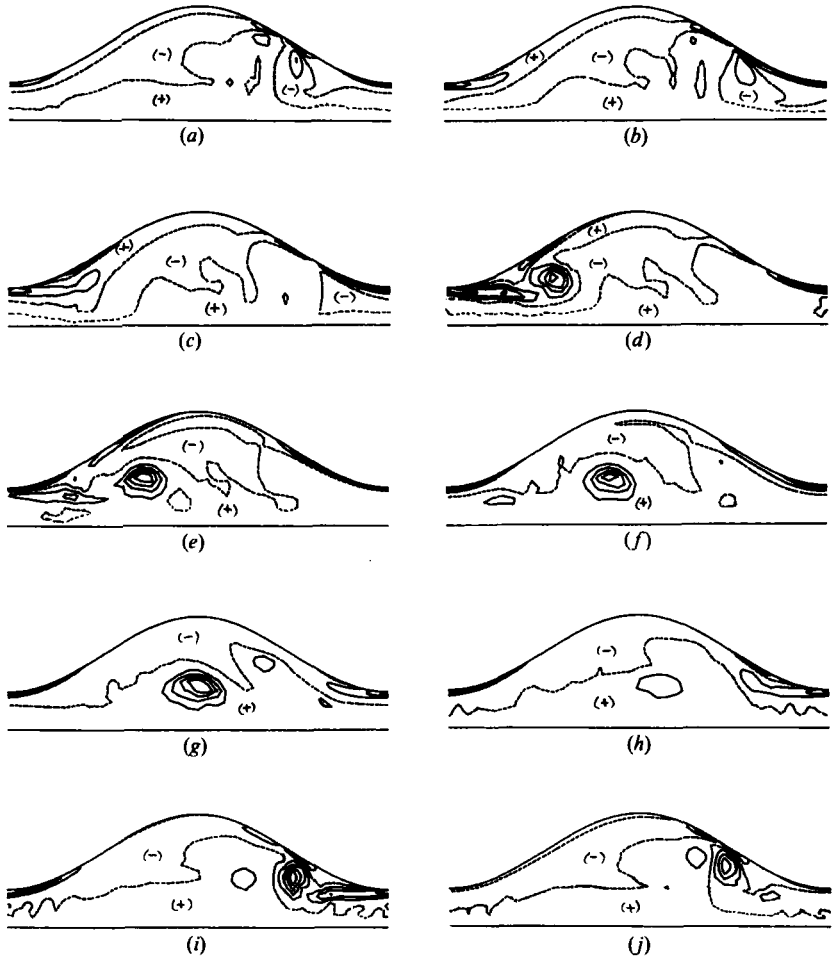

FIGURE 16. Computed vorticity contour plots for a flow with parameters $Re_0 = 300$, $St = 0.035$: (*a*)–(*j*) $t = 0.10$–1.00 in increments of 0.10: (*a*) $\Delta\zeta_+ = 3.29$, $\Delta\zeta_- = -2.63$; (*b*) 2.64, −1.50; (*c*) 2.61, −1.33; (*d*) 1.17, −1.31; (*e*) 1.02, −0.85; (*f*) 0.87, −1.93; (*g*) 0.66, −2.88; (*h*) 1.48, −2.61; (*i*) 2.04, −1.23; (*j*) 2.65, −1.65.

of the sense of asymmetry is different in each case. In the computations it is the sense of flow as the calculation is initiated which determines the sense of asymmetry, and this suggests that a stabilizing process of the kind described above can occur after the initial stroke has filled the tube with vorticity of a particular sign. In the experiments on the other hand, the sense of asymmetry is fixed relative to the test section, irrespective of the start-up conditions. Hence it appears that slight irregularities in the shape of the test section cause slightly more vorticity of a particular sign to be generated, and that this gives rise to asymmetry when coupled with a reinforcing mechanism.

These suggestions regarding the causes of time asymmetries are consistent with the discrepancy in Reynolds-number thresholds between the experiments and computations. If we consider a set of flow parameters giving rise to symmetric flow in the computations and asymmetric flow experimentally, for example that represented in figure 14(*a*)(iii), it can be seen that the computed flow is almost stably asymmetric

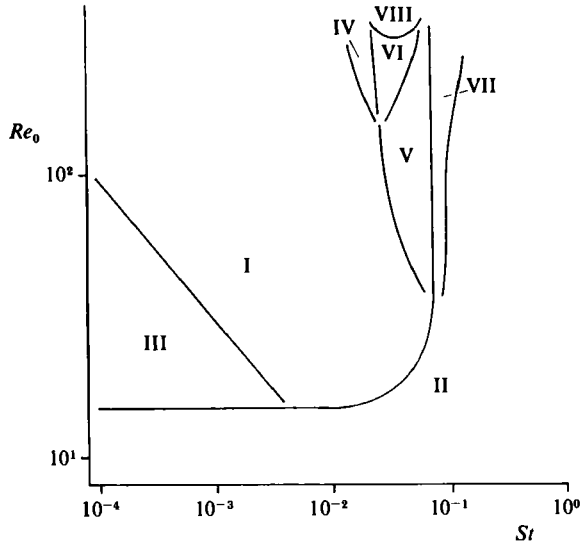

FIGURE 17. Predicted occurrence of flow structures in the (Reynolds number)–(Strouhal number) plane. The Roman numerals identify the different flow structures described in the text.

for a number of cycles before the asymmetry begins to decay rapidly. The slight additional imposed asymmetry of the experiments is sufficient to render such flows stably asymmetric.

7. Occurrence of flow structures in the Reynolds number–Strouhal number plane

In §§4–6 several flow structures have been described, but the ranges of parameter values for which these flows occur has not been indicated in any systematic way: this is done in the present section. The regions of the (Reynolds number)–(Strouhal number) plane in which the various flows have been predicted to occur numerically are shown in figure 17. The flow structures identified in the figure are as follows:

Type I: inertial vortex ejected during bulk-flow reversal (as described in Sobey 1980 and shown in figure 3);

Type II: viscous-dominated flows (as described in Sobey 1980);

Type III: quasi-steady flow (as described in Sobey 1983);

Type IV: the flow structure shown in figure 4;

Type V: the flow structure shown in figure 7;

Type VI: the flow structure shown in figure 11;

Type VII: the flow structure shown in figure 12;

Type VIII: any time-asymmetric flow, as shown in figure 15, for example.

Note that the curves bounding the type-II and type-III flows represent a similar division of the parameter space to that shown in Sobey (1983).

The new flow structures described in §5 are found in the Strouhal-number range 0.02–0.1, and these flows exhibit intricate streamline patterns which change in complex ways. At higher and lower Strouhal numbers the flow structures tend to be simpler. The reason for the existence of this Strouhal-number band of relatively complex flows is not clear, but it is perhaps significant that in this range the lengths

of typical particle paths, on the timescale of one flow cycle, are comparable with the wall wavelength.

The flow-visualization experiments have confirmed the existence of flow structure of types I, IV, V and VIII. These flows have usually been found in regions of the parameter space consistent with the computations, although a systematic comparison has not been carried out. The exception to this consistency lies in the more frequent occurrence of time asymmetries in the experiments, as already discussed: the experimental extent of time-asymmetric flows corresponds approximately to regions VI and VIII of figure 17 and that part of region V for which the Reynolds number is greater than 150.

8. Conclusions

A very important distinction between the new flow structures described in §§5 and 6 and those given in Sobey (1980, 1983) is the increased dependence of the flow development in any half-cycle on events in the preceding half-cycle. Sobey (1980) states that, in the inertially dominated flows he considers, the velocity field existing at any instant of zero flow has little effect on the flow in the subsequent half-cycle. This is clearly not the case for many of the flows described here, in which a recirculation may persist long after mean flow reversal. The increasing importance of time-history effects has been explained in terms of both an increase in the strength of recirculations as the Strouhal number and Reynolds number change, and a decrease in those physical processes tending to cause smoothing of the vorticity field, that is convection and diffusion of vorticity.

When time-history effects are important, the possibility of time asymmetry exists. Since the asymmetries described in §6 can occur in either of two senses, dependent on the initial direction of flow (in the computations) or small perturbations of the wall shape (in the experiments), their occurrence can be regarded as a bifurcation of the flow structure in the parameter space. The emergence of a flow in which the periodicity of the velocity field is equal to three complete cycles of the variation in flow rate [see figure 14*b*(iv)] suggests that further bifurcations can occur. In addition, the apparently random behaviour of χ, the measure of time asymmetry, shown in figure 14*b*(v) is strongly suggestive of transition to turbulence. These facts argue for a detailed study of the bifurcation diagram in this region of the parameter space, with the possibility that the results may improve our understanding of transitional flows.

I am greatly indebted to Dr I. J. Sobey of Schlumberger Research, Cambridge, for invaluable assistance and encouragement throughout this work. I would also like to thank all members of the Medical Engineering Unit of Oxford University where this work was performed, including Drs B. J. Bellhouse, J. W. Stairmand and J. P. G. Urban for useful advice, and M. A. L. Stevenson, G. Walker, J. Greenford and R. W. H. Lewis for technical assistance. Thanks are also due to the referees for many valuable criticisms and suggestions. I acknowledge receipt of a Science and Engineering Research Council postgraduate studentship.

REFERENCES

Batchelor, G. K. 1967 *An Introduction to Fluid Dynamics*. Cambridge University Press.

Bellhouse, B. J., Bellhouse, F. H., Curl, C. M., MacMillan, T. I., Gunning, A. J., Spratt, E. H., MacMurray, S. B. & Nelems, J. M. 1973 A high efficiency membrane oxygenator and pulsatile pump and its application to animal trials. *Trans. Am. Soc. Artif. Int. Organs* **19**, 72–79.

Bellhouse, B. J. & Snuggs, T. A. 1977 Augmented mass transfer in a membrane lung and a hemodialyser using vortex mixing. *INSERM-Euromech 92*, **71**, 371–384.

Cheng, L. C., Clark, M. E. & Robertson, J. M. 1972 Numerical calculations of oscillatory flow in the vicinity of square wall obstacles in plane conduits. *J. Biomech.* **5**, 467–484.

Cheng, L. C., Robertson, J. M. & Clark, M. E. 1973 Numerical calculations of oscillatory non-uniform flow. II. Parametric study of pressure gradient and frequency with square wall obstacles. *J. Biomech.* **6**, 521–538.

Daly, B. J. 1975 A numerical study of pulsatile flow through constricted arteries. *Proc. 4th Intl Conf. on Num. Methods in Fluid Dyn.* Lecture Notes in Physics, vol. 35, pp. 117–124. Springer.

Daly, B. J. 1976 A numerical study of pulsatile flow through stenosed canine femoral arteries. *J. Biomech.* **9**, 465–475.

Gillani, N. V. & Swanson, W. M. 1976 Time-dependent laminar flow through a spherical cavity. *J. Fluid Mech.* **78**, 99–127.

Hall, P. 1974 Unsteady viscous flow in a pipe of slowly varying cross-section. *J. Fluid Mech.* **64**, 209–226.

Lyne, W. H. 1971 Unsteady viscous flow over a wavy wall. *J. Fluid Mech.* **50**, 33–48.

O'Brien, V. 1975 Unsteady separation phenomena in a two-dimensional cavity. *AIAA J.* **13**, 415–416.

Ralph, M. E. 1985 Flows in wavy-walled tubes. D.Phil. thesis, University of Oxford.

Roache, P. J. 1976 *Computational Fluid Dynamics*, 2nd edn. Hermosa.

Savvides, G. N. & Gerrard, J. H. 1984 Numerical analysis of the flow through a corrugated tube with the application to arterial prosthesis. *J. Fluid Mech.* **138**, 129–160.

Sobey, I. J. 1980 On flow through furrowed channels. Part 1. Calculated flow patterns. *J. Fluid Mech.* **96**, 1–26.

Sobey, I. J. 1982 Oscillatory flow at intermediate Reynolds number in asymmetric channels. *J. Fluid Mech.* **125**, 359–373.

Sobey, I. J. 1983 The occurrence of separation in oscillatory flow. *J. Fluid Mech.* **134**, 247–257.

Stephanoff, K. D., Sobey, I. J. & Bellhouse, B. J. 1980 On flow through furrowed channels. Part 2. Observed flow patterns. *J. Fluid Mech.* **96**, 27–32.